NANO LETTERS

pubs.acs.org/NanoLett Letter

A Bioinspired Artificial Gustatory Neuron for a Neuromorphic Based Electronic Tongue

Joon-Kyu Han,[§] Sang-Chan Park,[§] Ji-Man Yu, Jae-Hyuk Ahn,* and Yang-Kyu Choi*

Cite This: *Nano Lett.* 2022, 22, 5244−5251 Read Online

ACCESS | Metrics & More | Article Recommendations | Supporting Information

ABSTRACT: A novel biomimicked neuromorphic sensor for an energy efficient and highly scalable electronic tongue (E-tongue) is demonstrated with a metal-oxide-semiconductor field-effect transistor (MOSFET). By mimicking a biological gustatory neuron, the proposed E-tongue can simultaneously detect ion concentrations of chemicals on an extended gate and encode spike signals on the MOSFET, which acts as an input neuron in a spiking neural network (SNN). Such in-sensor neuromorphic functioning can reduce the energy and area consumption of the conventional E-tongue hardware. pH-sensitive and sodium-sensitive artificial gustatory neurons are implemented by using two different sensing materials: Al_2O_3 for pH sensing and sodium ionophore X for sodium ion sensing. In addition, a sensitivity control function inspired by the biological sensory neuron is demonstrated. After the unit device characterization of the artificial gustatory neuron, a fully hardware-based E-tongue that can classify two distinct liquids is demonstrated to show a practical application of the artificial gustatory neurons.

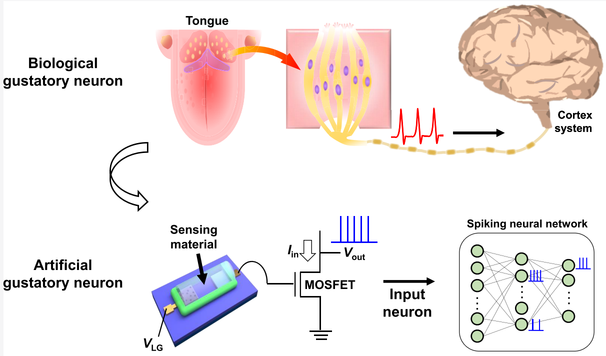

KEYWORDS: *Biosensor, electronic tongue, gustatory neuron, neuromorphic, spiking neural network (SNN)*

In a biological gustatory system, tastes are identified by a composite of responses from the gustatory receptor neurons located at taste buds.[1−3] The combined signals from the gustatory receptor neurons are transported to the gustatory cortex in the brain for identifying a distinct pattern of each taste, as illustrated in Figure 1a. Mimicking the biological gustatory system, an electronic tongue (E-tongue) has been developed with a decoupled sensor array and a separated pattern recognition system (Figure S1), which corresponds to gustatory receptor neurons and the gustatory cortex, respectively.[4−6] Because a deep neural network (DNN) has been adopted for accurate identification of the various complicated solutions, the E-tongue with the aid of the DNN is applicable to a field of fresh food monitoring, sweat analysis, medical applications, pharmaceutical industries, and environmental monitoring.[7−11]

However, heavy hardware and large energy consumption impede practical use because a powerful computer is required for the implementation of the DNN. Application to IoT and mobile devices, which are currently the most important fields of sensors, becomes difficult. One possible solution is adopting all-in-one neuromorphic sensor system based on a spiking neural network (SNN), which consumes less energy owing to data transmission with spikes and data in movement between a central processing unit (CPU) and memory.[12−16] In addition, heavy hardware components such as an analog-to-digital converter (ADC) for converting sensor data into an appropriate digital form are not required. Due to this low energy consumption and small hardware cost, the neuromorphic sensor system to do sensing and neuronal functioning is advantageous for mobile and IoT sensors. The first step for realizing the SNN is to change continuous and analog environmental signals to discrete spike signals. In the biological gustatory system, gustatory receptor neurons perform these functions, but general sensors cannot be applied owing to the lack of a spike encoding function. Therefore, a new device concept should be developed to combine the sensing and the neuronal functioning. Recently, artificial photoreceptors and mechanoreceptors that can concurrently perform sensing and spike encoding for in-sensor neuromorphic functioning were demonstrated for visual sensory and tactile sensory systems, respectively. However, a device that can simultaneously detect ion concentrations and generate spike signals for an E-tongue has not been developed yet (Table S1).[17−20]

Sensitivity control of the biological gustatory neuron is typically performed in the gustatory sensory system.[21,22] When gustatory neurons are continually exposed to a certain chemical, the sensitivity decreases, which is a kind of neural

Received: March 18, 2022
Revised: June 20, 2022
Published: June 23, 2022

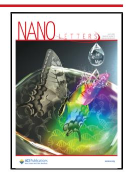

https://doi.org/10.1021/acs.nanolett.2c01107
Nano Lett. 2022, 22, 5244−5251

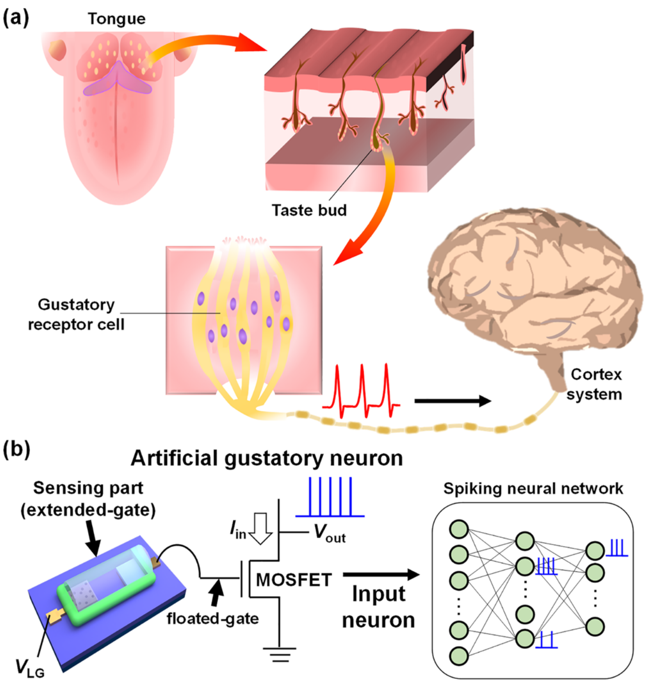

Figure 1. Biological gustatory system and proposed neuromorphic E-tongue system with artificial gustatory neuron. (a) Action potentials are generated in the gustatory receptor neuron according to the chemicals, in order to transport the spike signals to the brain for neural processing in the biological gustatory system. (b) Spike signals are generated in the artificial gustatory neuron according to the chemicals, which can act as an input neuron in a neuromorphic E-tongue based on a spiking neural network (SNN). The artificial gustatory neuron has a structure of a MOSFET with an extended-gate biosensor, where the sensing part (bioreceptor) is electrically connected but physically separated with the MOSFET. In the sensing part, a sensing layer is located between two electrodes. While one electrode is connected to the MOSFET, the other electrode is used for a liquid-gate terminal, where the electrical bias is applied through the liquid.

adaptation. Such neuronal adaptation is critical for improving sensory perception by producing a signal contrast with other neurons. Furthermore, energy efficiency can be improved by inhibiting the unnecessary neurons. However, such sensitivity control cannot be achieved with conventional biosensors.

In this work, an artificial gustatory neuron to do the sensing and neuronal functioning is demonstrated for a neuromorphic-based E-tongue as a one-body type sensory neuron. Gustatory neurons in two taste buds, sour and salty, are imitated using a metal-oxide-semiconductor field-effect transistor (MOSFET) that has an extended gate to be served as a bioreceptor like an antenna to collect a taste source. Simultaneous sensing and spike encoding in the sensor are achieved, where the spiking frequency is changed according to the concentrations of hydrogen and sodium ions. This artificial gustatory neuron acts as an input neuron for the SNN, as illustrated in Figure 1b. A highly scalable and energy efficient one-body type E-tongue for mobile and IoT applications can be implemented due to the neuromorphic architecture where the data are transmitted with spikes and heavy hardware components such as an ADC, CPU, and memory are not required (Figure S1). By changing the electrical gate potential of the MOSFET-based extended-gate biosensors, sensitivity control of the biological sensory neuron for neuronal adaptation is imitated with the artificial gustatory neuron. Beyond the characterization of the unit device, a SNN that can classify two liquids is constructed with synaptic devices in order to demonstrate a practical application of the artificial gustatory neurons to an E-tongue.

A MOSFET-based extended-gate biosensor, where the sensing part is physically separated from the channel region of the MOSFET but electrically connected to a gate of the MOSFET, was adopted for an artificial gustatory neuron, as shown in Figure 1b.[23,24] It should be noted that the sensing part has a two-terminal structure where a sensing layer is located between two electrodes. While one electrode is connected to the MOSFET gate, the other electrode acts as a liquid gate for applying the electrical bias (liquid-gate voltage, V_{LG}) through the ionic solution. For the pH sensor, hydrogen ions reversibly bound on the oxide layer are served as the surface charges, which are converted to the surface potential based on the Nernst equation. The surface potential and floated-gate voltage of the MOSFET are changed by surface charges produced by the ionic solution on the sensing layer of the extended gate. This can change the various electrical characteristics of the MOSFET including the threshold voltage (V_T) in the transfer characteristic, latch-up voltage (V_{latch}) in the output characteristic, and firing threshold voltage ($V_{T,firing}$) and spiking frequency (f) in the neuronal characteristic. The detailed operation mechanism of the artificial gustatory neuron will be discussed later.

A MOSFET that has a channel width (W) of 350 nm and a gate length (L_G) of 580 nm was fabricated on a silicon on insulator (SOI) wafer, as shown in Figure 2a. It should be

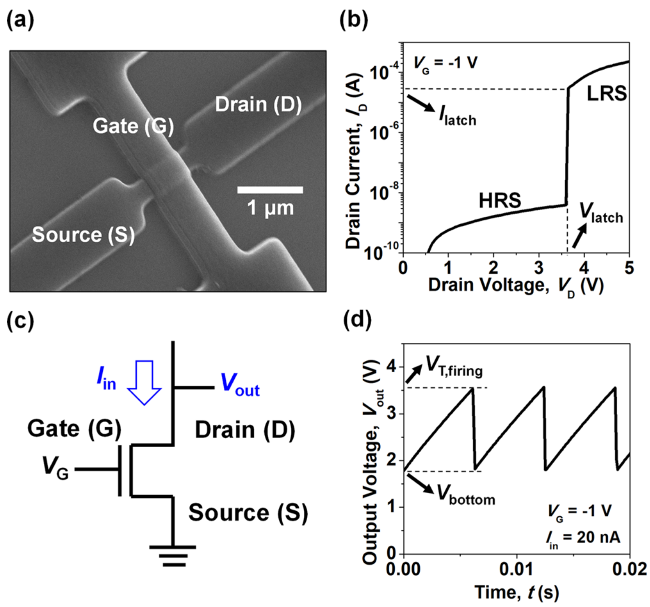

Figure 2. Characteristics of a MOSFET without the sensing part. (a) Scanning electron microscope (SEM) image of the MOSFET that was fabricated on a SOI wafer to enable the single transistor latch (STL) and the neuronal operation. (b) Output characteristic (I_D-V_D) of the MOSFET. A high resistance state (HRS) instantly changed to a low resistance state (LRS) when the drain voltage (V_D) reached the latch-up voltage (V_{latch}) due to the STL phenomenon. (c) Neuronal operation schematic of the MOSFET. Input current (I_{in}) is applied to the drain and the output voltage (V_{out}) is measured in the same drain. (d) Spiking characteristic (V_{out}-t) of the MOSFET. The output voltage (V_{out}) was reduced instantly when V_{out} reached the firing threshold voltage ($V_{T,firing}$) because of neuronal firing.

https://doi.org/10.1021/acs.nanolett.2c01107
Nano Lett. 2022, 22, 5244−5251

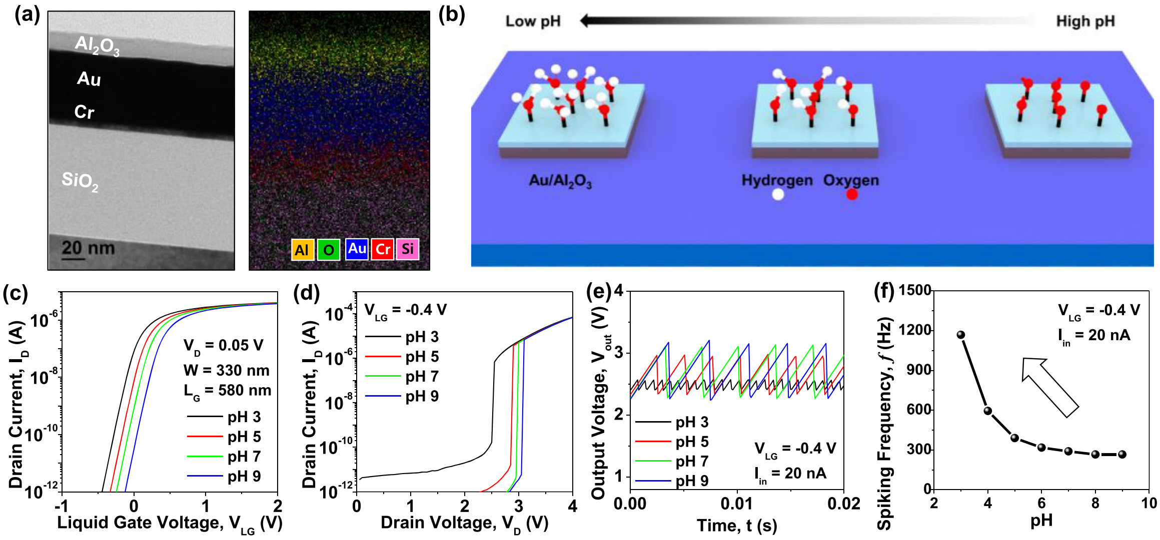

Figure 3. pH-sensitive artificial gustatory neuron. (a) (left) Transmission electron microscope (TEM) image of the pH sensing layer, where it was confirmed that the 15 nm thick Al_2O_3 layer was well deposited. (right) Energy dispersive spectroscopy (EDS) mapping, in which the Al peak (yellow) and O peak (green) were confirmed. (b) Schematic illustration of the principle of the pH sensing response to hydrogen ions. Surface charges are generated, and the surface potential is changed when hydrogen ions reversibly attach to the active OH sites on the Al_2O_3 surface. (c) Transfer characteristics (I_D-V_{LG}) and (d) output characteristics (I_D-V_D) of the fabricated artificial gustatory neuron response to pH. Threshold voltage (V_T) and latch-up voltage (V_{latch}) shifted leftward at a decreased pH value of the solution. (e) Spiking characteristics (V_{out}-t). Firing threshold voltage ($V_{T,firing}$) decreased and the bottom voltage (V_{bottom}) increased as the pH value decreased. (f) Spiking frequency (f) as a function of the pH value. f increased at a lower pH value, which is a desired property of the pH-sensitive artificial gustatory neuron.

noted that the floating body on the SOI wafer can enable single transistor latch (STL) and neuronal operation.[15,16] The fabrication processes of the MOSFET are explained in methods/experiment section and Supporting Information (Figure S2).

Figure 2b shows the output characteristics of the fabricated MOSFET, represented by the drain current (I_D) versus the drain voltage (V_D). When V_D reached the latch-up voltage (V_{latch}), a high resistance state (HRS) rapidly changed to a low resistance state (LRS) by the STL phenomenon, where I_D abruptly increased. This property allows mimicking of the integrate-and-fire (IF) behavior of a biological neuron even with a single MOSFET.[15,16] In detail, when constant input current (I_{in}) is applied to the drain electrode and the output voltage (V_{out}) is measured in the same drain electrode, as illustrated in Figure 2c, V_{out} increases because the inserted charges cannot flow out toward the source, and the charges are integrated in the drain parasitic capacitor. When V_{out} reaches the V_{latch}, which is the same as the firing threshold voltage ($V_{T,firing}$) in neuronal operation, the integrated charges instantly flow out toward the source. Furthermore, the fired charges can be detected from the output current (I_{out}) measured at the source, which is determined by the latch-up current (I_{latch}).[15] When constant I_{in} is applied, this IF operation is repeated to generate continuous spiking, as shown in Figure 2d. While $V_{T,firing}$ is determined by V_{latch}, the bottom voltage (V_{bottom}) of the spiking is determined by I_{latch}.[25] For a lower I_{latch}, V_{bottom} becomes higher because fewer integrated charges are able to escape from the drain parasitic capacitor.

The spiking frequency (f) of the IF neuron based on the single MOSFET can be expressed as follows:

$$f = \frac{I_{in}}{C_{par}(V_{T,firing} - V_{bottom})} \quad (1)$$

where C_{par} represents the parasitic capacitance including the drain junction capacitance, pad capacitance, and equipment capacitance including the cable capacitance.[19,20] From the above equation, f tends to be increased when $V_{T,firing}$ decreases and V_{bottom} increases. By adjustment of $V_{T,firing}$ and V_{bottom} with the sensing part (extended-gate) of the artificial gustatory neuron, f is tunable to mimic biological gustatory neurons. It should be noted that C_{par} in our measurement system was fixed as 74 pF.

A pH-sensitive artificial gustatory neuron (abbreviated as a pH-sensitive neuron) was realized by connecting a pH sensing part to the MOSFET as an extended-gate structure. The pH sensing part was fabricated on a highly p-doped silicon wafer with a top 90 nm thick SiO_2 as the starting material.[26] The fabrication process is explained in the methods/experimenT section and Supporting Information (Figure S3). Figure 3a shows a transmission electron microscope (TEM) image, where it was confirmed that the Al_2O_3 layer to detect pH was well deposited on the Au electrode, and energy dispersive spectroscopy (EDS) mapping overlaid with the TEM image showed the Al peak (yellow) and O peak (green) clearly.

Figure 3b shows the working principle of the pH sensing of the MOSFET-based extended-gate biosensor. As the pH value of the buffer solution decreases, more hydrogen ions reversibly bind to the active OH sites of the Al_2O_3 surface, and the surface charge and surface potential are increased. In detail, the surface charge on the sensing electrode becomes positive due to hydrogen ions bound on the active OH sites, compared with a point of zero charge. Therefore, as shown in the transfer characteristics of Figure 3c, which are represented by the drain current versus liquid-gate voltage (I_D-V_{LG}) curve, V_T was shifted leftward because of the increased surface potential and floated-gate voltage of the MOSFET, following the Nernst equation (Figure S4a).[26−28] The change in surface charge and surface potential also affects the STL observed in the output

https://doi.org/10.1021/acs.nanolett.2c01107
Nano Lett. 2022, 22, 5244−5251

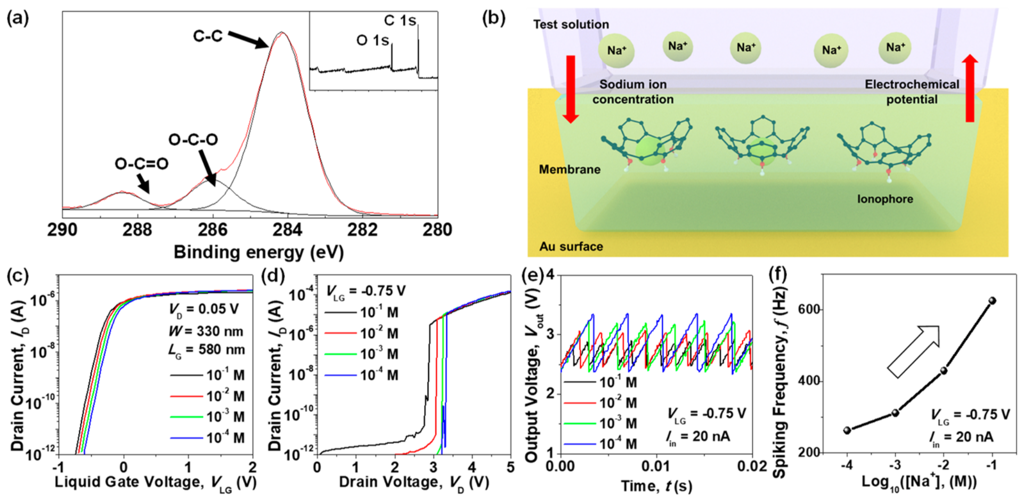

Figure 4. Sodium-sensitive artificial gustatory neuron. (a) X-ray Photoelectron Spectroscopy (XPS) spectra of a sodium ionophore X in the sodium sensing layer: the inset shows the XPS survey scan where O 1s and C 1s peaks were confirmed; C 1s core scan where the O−C═O peak to capture sodium ions was confirmed. (b) Schematic illustration of the origin of the sodium sensing response to the sodium ions. As the sodium-selective ionophore captures sodium ions, membrane potential is generated due to the concentration difference of the membrane and solution interface. (c) Transfer characteristics (I_D-V_{LG}) and (d) output characteristics (I_D-V_D) of the fabricated artificial gustatory neuron response to sodium ions. Threshold voltage (V_T) and latch-up voltage (V_{latch}) shifted leftward when the solution had an increased sodium concentration. (e) Spiking characteristics (V_{out}-t). Firing threshold voltage ($V_{T,firing}$) decreased and bottom voltage (V_{bottom}) increased in higher sodium concentration. (f) Spiking frequency (f) as a function of the sodium concentration. f increased as the sodium concentration increased, which is a desired property of the sodium-sensitive artificial gustatory neuron.

characteristic, which is represented as the I_D-V_D curve. When the floated-gate voltage of the MOSFET increases by the increased surface charge and surface potential, the number of carriers injected from the source to the body and the impact ionization rate in the body increase because of the reduced energy barrier between the source and the body, which is known as the built-in potential at a pn junction. Therefore, V_{latch} and I_{latch} were decreased at lower pH values, as shown in Figure 3d.

Figure 3e shows the neuronal spiking operation represented by the $V_{out}-t$ curve, when constant I_{in} was applied to the drain electrode and V_{out} was measured in the same drain electrode. Since V_{latch} and I_{latch} determine $V_{T,firing}$ and V_{bottom}, respectively, $V_{T,firing}$ decreased and V_{bottom} increased at a lower pH value to increase f, as shown in Figure 3e,f. As a result, the spiking was activated as the pH value of the solution decreased, which is the representative property of acid sensing gustatory receptor neurons.[29] When V_{LG} of −0.4 V was applied to the liquid gate, f was increased by 902 Hz when the pH value decreased from 9 to 3. The average sensitivity was extracted as 150 Hz/pH in the range of pH 3−9.

The sensitivity can be expressed as follows from eq 1:

$$\frac{df}{dpH} = \frac{I_{in}}{C_{par}}\frac{d}{dpH}\left(\frac{1}{V_{T,firing} - V_{bottom}}\right) \quad (2)$$

Note that I_{in} and C_{par} are not a function of pH because they are fixed by the measurement setup.

In a biological gustatory neuron, control of the sensitivity is typically performed.[21,22] For example, when the gustatory neurons are continuously exposed to a certain chemical, the sensitivity becomes smaller by neuronal adaptation. Such neuronal adaptation is important to enhance sensory perception by creating a signal contrast with other gustatory neurons. In addition, energy efficiency can be enhanced by inhibiting the response of the useless neurons. From eq 2, the sensitivity can be controlled with V_{LG}, which determines the $\frac{d}{dpH}\left(\frac{1}{V_{T,firing} - V_{bottom}}\right)$ term, when I_{in} and C_{par} are fixed. For example, the sensitivity can be reduced by decreasing V_{LG} to −0.6 V, as shown in Figure S5a. As V_{LG} decreases, the energy barrier between the source and the body increases. As a consequence, the increase of the number of carriers injected from the source to the body is not sufficient to increase the impact ionization rate and decrease V_{latch} although more hydrogen ions bind to the Al_2O_3 surface. In other words, $\frac{d}{dpH}\left(\frac{1}{V_{T,firing} - V_{bottom}}\right)$ decreases with a smaller V_{LG}. As a result, the sensitivity of the artificial gustatory neuron reduces by decreasing V_{LG}. Note that such biomimicking sensitivity control is difficult to achieve in the conventional biosensor that uses V_T as a sensing metric.

Next, the energy consumption of the pH-sensitive neuron was evaluated. As shown in Figure S6a, the energy per spike (E/spike) was extracted as 42.5 pJ/spike at a pH of 3, and it was increased as the pH value of the solution increased because of the elevated $V_{T,firing}$. In addition, the average power consumption (P_{avg}) in one spike was extracted as 49.6 nW at pH of 3. Considering that P_{avg} of the conversion circuit (ADC) to convert the analog sensor data into the digital domain is in the range of a few μW, the artificial gustatory neuron can greatly reduce the energy consumption of the E-tongue, although P_{avg} includes the power consumption in the sensor.[30]

A sodium-sensitive artificial gustatory neuron (abbreviated as a sodium-sensitive neuron) was realized by connecting a sodium sensing part to the MOSFET as an extended-gate structure. The sodium sensing part was also fabricated on a highly p-doped silicon wafer with a top 90 nm thick SiO_2 as the starting material.[31] The fabrication process is explained in the methods/experiment section and Supporting Information (Figure S3). For an analysis of sodium ionophore X, X-ray photoelectron spectroscopy (XPS) was used. An inset of

https://doi.org/10.1021/acs.nanolett.2c01107
Nano Lett. 2022, 22, 5244−5251

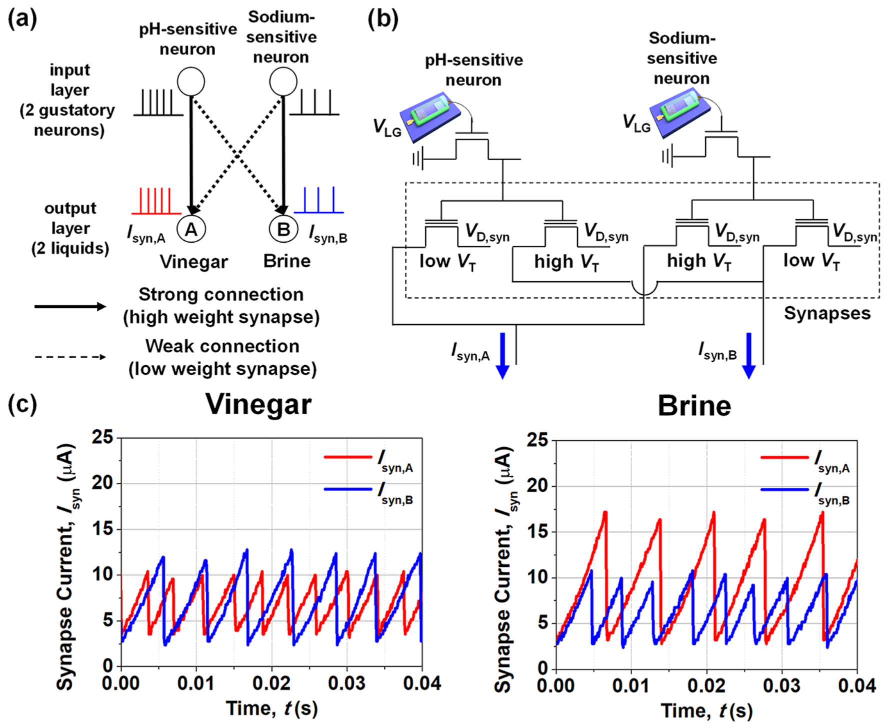

Figure 5. Liquid classification with E-tongue. (a) Spiking neural network (SNN) based on a single-layer perceptron for the classification of two liquids. The input layer and the output layer corresponded to the two artificial gustatory neurons (pH-sensitive neuron and sodium-sensitive neuron) and the two liquids (vinegar and brine), respectively. (b) Circuit diagram for the E-tongue hardware. Electrical signals from the artificial gustatory neurons were transported to the synapses, which have a homotypic structure with the MOSFET comprising the artificial gustatory neuron. The weight of the synapses was modulated by changing the threshold voltage (V_T) of the MOSFET with charge trapping in the silicon nitride (Si_3N_4) charge trap layer. Drain voltage applied to the synapses ($V_{D,syn}$) was set as 1 V. (c) Synapse current measured at output layer A ($I_{syn,A}$) and output layer B ($I_{syn,B}$). When the liquid was vinegar, the spiking frequency of $I_{syn,A}$ was larger than $I_{syn,B}$. Otherwise, $I_{syn,B}$ had a larger spiking frequency than $I_{syn,A}$ when the liquid was brine.

Figure 4a shows that the XPS spectra reveal two peaks at 284.46 and 532.36 eV, respectively. One peak at 284.46 eV corresponds to the C 1s peak and another at 532.36 eV corresponds to the O 1s peak where all atomic % closely matched the theoretical value of sodium ionophore X: specifically, the peak at 298.03 eV corresponds to the chemical state O−C═O, which could capture a sodium ion, as shown Figure 4a.[32] The working principle of the sodium ion sensing of the MOSFET-based extended-gate biosensor is illustrated in Figure 4b. As the sodium-selective ionophore captures sodium ions, the membrane potential is generated due to the concentration difference of the membrane/solution interface. Therefore, the I_D-V_{LG} curve was shifted leftward as the sodium concentration increased, as shown in Figure 4c. In addition, Figure 4d shows that V_{latch} and I_{latch} were reduced at higher sodium concentrations, similar to the pH sensing characteristics. Subsequently, as shown in Figure 4e, $V_{T,firing}$ and V_{bottom} decreased and increased, respectively. As a result, the spiking was activated as the sodium concentration increases such as the biological salt sensing gustatory receptor neurons, as shown in Figure 4f.[33] It should be noted that V_{LG} of −0.75 V was applied to the liquid gate for Figure 4d−f. The average sensitivity was extracted as 120 Hz/dec in the range of 10^{-4}–10^{-1} M. As observed for the pH-sensitive neurons, the sensitivity could be reduced by decreasing V_{LG} to −1 V, as shown in Figure S5b. *E*/spike and P_{avg} were also extracted for the sodium-sensitive neuron, as shown in Figure S6b.

We constructed the E-tongue hardware for liquid classification to demonstrate further applicability of the artificial gustatory neurons. Figure 5a shows the single-layer perceptron (SLP) neural network designed to classify two liquids: vinegar and brine. An input layer was composed of two artificial gustatory neurons and an output layer was composed of two nodes (A and B), which corresponded to two liquids. One artificial gustatory neuron was the pH-sensitive neuron illustrated in Figure 3, and the other was the sodium-sensitive neuron explained in Figure 4. The pH-sensitive neuron was strongly connected to output node A with high synaptic weight, while it was weakly connected to output node B with weak synaptic weight. Otherwise, output layer B was strongly connected to the sodium-sensitive neuron. Figure 5b shows the circuit diagram to realize the SNN with hardware. Other MOSFETs were utilized for synaptic devices that determine the synaptic weight between the input layer and the output layer, which have a homotypic structure with the MOSFET comprising the artificial gustatory neuron.[34,35] The detailed explanation of the synaptic devices is provided in Figure S7.

The electrical spiking signals from the artificial gustatory neurons (Figure S8) were transferred to the gate of the synaptic devices. It should be noted that V_{LG} of −0.8 V was applied to the pH-sensitive neuron and V_{LG} of −1 V was applied to the sodium-sensitive neuron. Finally, we measured the synapse current collected at output layer A ($I_{syn,A}$) and output layer B ($I_{syn,B}$) in order to classify vinegar and brine according to where the spiking frequency is higher between $I_{syn,A}$ and $I_{syn,B}$. In detail, a liquid was classified as vinegar when the spiking frequency of $I_{syn,A}$ was higher, and it was classified as brine when the spiking frequency of $I_{syn,B}$ was higher. As a

https://doi.org/10.1021/acs.nanolett.2c01107
Nano Lett. 2022, 22, 5244−5251

result, an E-tongue composed of the artificial gustatory neuron was demonstrated for the classification of two liquids. Although we implemented a very simple classification, more sophisticated classification of various liquids can be performed by increasing the number of hidden layers in the SNN instead of the SLP or by using multiple states of the synaptic devices (Figure S7d) instead of binary states.

In this paper, we demonstrated an artificial gustatory neuron for an energy and area efficient neuromorphic based E-tongue. The biological gustatory neuron was mimicked with a MOSFET-based extended-gate biosensor, where the neuronal spiking varied according to the ion concentrations of the solution. The proposed artificial gustatory neuron can simultaneously perform sensing and spike encoding that is adequate for the input neuron of the SNN located in the sensor module. By removing energy and area consuming signal transducers such as ADCs, it can greatly decrease energy consumption and hardware cost. Furthermore, because of the bioinspired neuromorphic architecture, hardware components of the von Neumann computer such as CPU and memory are not required, which can also dramatically lower energy consumption and hardware cost. As well as sensing and spiking encoding functions, sensitivity control mimicking the neuronal adaptation of the biological sensory neuron in order to enhance sensory perception and energy efficiency was presented. Artificial gustatory neurons that responded to hydrogen and sodium ions were demonstrated, and two liquids (vinegar and brine) were classified by construction of a SNN. The proposed artificial gustatory neuron will open a new avenue of E-tongues for mobile and IoT applications, which require low energy consumption and small hardware cost. In addition, artificial gustatory neurons without any structural modification can also be utilized to sense other tastes such as sweetness and bitterness by replacing the pH or sodium sensing layer with other sensing layers.

EXPERIMENTAL SECTION

Fabrication of a MOSFET. A MOSFET was fabricated on a p-type (100) silicon on insulator (SOI) wafer. After patterning the active silicon area, gate dielectrics composed of $SiO_2/Si_3N_4/SiO_2$ and a gate electrode composed of n^+ polycrystalline silicon (poly-Si) were sequentially deposited then patterned. Afterward, a gate side wall spacer was formed. Next, ion implantation with arsenic and rapid thermal annealing (RTA) were performed to make the source and drain electrodes. A nominal dimension of the used MOSFET is a channel width (W) of 350 nm and a gate length (L_G) of 580 nm. The detailed fabrication processes are explained in Supporting Information (Figure S2).

Fabrication of the Sensing Part (Extended Gate) for pH Detection. The pH sensing part was fabricated on a highly p-doped silicon wafer as a starting material. First, a thick SiO_2 of 90 nm was thermally grown. Second, a pair of electrodes (Cr/Au = 3 nm/50 nm) were patterned by three sequential processes: photolithography, metal deposition with an electron-beam (e-beam) evaporator, and metal lift-off. Third, an Al_2O_3 layer of 15 nm was deposited to sense a pH level by using another e-beam evaporator and globally patterned with a low resolution by a Kapton tape. A reference electrode was formed by drop-casting the Ag/AgCl ink (011464, ALS Co.) on the other Au electrode followed by drop-casting a polyvinyl butyral (PVB) solution. The PVB solution was prepared by dissolving 395.5 mg of PVB and 50 mg of NaCl into 5 mL of methanol. Before the first measurement, the reference electrode was preconditioned by a conditioning solution (3 M KCl) for 12 h.

Fabrication of the Sensing Part (Extended Gate) for Sodium Detection. The sodium sensing part was also fabricated on a highly p-doped silicon wafer as a starting substrate. Afterward, a thick SiO_2 of 90 nm was thermally grown. Next, a pair of electrodes (Cr/Au = 3 nm/50 nm) were patterned by the same lift-off process, as mentioned above. And a reference electrode was fabricated by the same process described above. A sodium-selective membrane cocktail was composed of sodium ionophore X (1 wt %), polyvinyl chloride (PVC) (33 wt %), and bis(2-ethylhexyl) adipate (DOA) (66 wt %). The total 100 mg of this membrane cocktail was dissolved in 500 μL of tetrahydrofuran (THF). The sodium-selective membrane was deposited by the drop-cast method. Such drop-casting with a volume of approximately 10 μL was done to fully cover the electrode by use of a micropipette. Then, it was dried overnight in ambient conditions. The detailed fabrication processes for both the pH sensor and the sodium are explained in Supporting Information (Figure S3).

Electrical Characterization. Electrical characteristics were measured using a B1500A semiconductor parameter analyzer (Keysight).

SEM Analysis. SEM images were taken using a Magellan 400 field emission SEM (FEI Company).

TEM Analysis. TEM images were taken using a FE-STEM (HD-2300A) device made by Hitachi High-Technologies Corporation.

XPS Analysis. XPS analysis was conducted using a K-Alpha XPS system (Thermo Fisher Scientific Ltd.)

ASSOCIATED CONTENT

Supporting Information

The Supporting Information is available free of charge at https://pubs.acs.org/doi/10.1021/acs.nanolett.2c01107.

Comparison of conventional computing architecture-based electronic tongue and neuromorphic-based electronic tongue with artificial gustatory neuron; fabrication procedure of a MOSFET without the sensing part; fabrication procedure of the sensing part (extended gate); threshold voltage sensitivity of the MOSFET-based extended-gate biosensor; sensitivity control with liquid-gate voltage; evaluation of the energy consumption; synaptic device with silicon oxide−nitride-oxide−silicon (SONOS) MOSFET structure; output voltage (V_{out}) of the artificial gustatory neurons during liquid classification; comparison with previously reported artificial sensory neurons (PDF)

AUTHOR INFORMATION

Corresponding Authors

Jae-Hyuk Ahn − *Department of Electronics Engineering, Chungnam National University, Daejeon 34134, Republic of Korea*; Email: jaehyuk@cnu.ac.kr

Yang-Kyu Choi − *School of Electrical Engineering, Korea Advanced Institute of Science and Technology (KAIST), Daejeon 34141, Republic of Korea*; orcid.org/0000-0001-5480-7027; Email: ykchoi@ee.kaist.ac.kr

https://doi.org/10.1021/acs.nanolett.2c01107
Nano Lett. 2022, 22, 5244−5251

Authors

Joon-Kyu Han − *School of Electrical Engineering, Korea Advanced Institute of Science and Technology (KAIST), Daejeon 34141, Republic of Korea*

Sang-Chan Park − *Department of Electronics Engineering, Chungnam National University, Daejeon 34134, Republic of Korea*

Ji-Man Yu − *School of Electrical Engineering, Korea Advanced Institute of Science and Technology (KAIST), Daejeon 34141, Republic of Korea*

Complete contact information is available at: https://pubs.acs.org/10.1021/acs.nanolett.2c01107

Author Contributions

[§]J.-K.H. and S.-C.P. equally contributed to this work.

Notes

The authors declare no competing financial interest.

■ ACKNOWLEDGMENTS

This work was supported by National Research Foundation (NRF) of Korea, under Grants 2018R1A2A3075302, 2020M3F3A2A01082592, and 2020R1F1A106824, in part by the IC Design Education Center (EDA Tool and MPW).

■ REFERENCES

(1) Hallock, R.; Dilorenzo, P. Temporal Coding in the Gustatory System. *Neuroscience & Biobehavioral Reviews* **2006**, *30*, 1145−1160.
(2) Farbman, A. I. Fine Structure of the Taste Bud. *Journal of Ultrastructure Research* **1965**, *12*, 328−350.
(3) Trivedi, B. P. Gustatory System: The Finer Points of Taste. *Nature* **2012**, *486*, S2−S3.
(4) Toko, K. RETRACTED: Electronic Tongue. *Biosens. Bioelectron.* **1998**, *13*, 701−709.
(5) Jiang, H.; Zhang, M.; Bhandari, B.; Adhikari, B. Application of Electronic Tongue for Fresh Foods Quality Evaluation: A Review. *Food Reviews International* **2018**, *34*, 746−769.
(6) Podrażka, M.; Bączyńska, E.; Kundys, M.; Jeleń, P.; Witkowska Nery, E. Electronic Tongue—A Tool for All Tastes? *Biosensors* **2018**, *8*, 3.
(7) Ha, D.; Sun, Q.; Su, K.; Wan, H.; Li, H.; Xu, N.; Sun, F.; Zhuang, L.; Hu, N.; Wang, P. Recent Achievements in Electronic Tongue and Bioelectronic Tongue as Taste Sensors. *Sens. Actuators, B* **2015**, *207*, 1136−1146.
(8) Mimendia, A.; Gutiérrez, J. M.; Leija, L.; Hernández, P. R.; Favari, L.; Muñoz, R.; del Valle, M. A Review of the Use of the Potentiometric Electronic Tongue in the Monitoring of Environmental Systems. *Environmental Modelling & Software* **2010**, *25*, 1023−1030.
(9) Gutiérrez, M.; Alegret, S.; Cáceres, R.; Casadesús, J.; Marfà, O.; del Valle, M. Nutrient Solution Monitoring in Greenhouse Cultivation Employing a Potentiometric Electronic Tongue. *J. Agric. Food Chem.* **2008**, *56*, 1810−1817.
(10) Tønning, E.; Sapelnikova, S.; Christensen, J.; Carlsson, C.; Winther-Nielsen, M.; Dock, E.; Solna, R.; Skladal, P.; Nørgaard, L.; Ruzgas, T.; et al. Chemometric Exploration of an Amperometric Biosensor Array for Fast Determination of Wastewater Quality. *Biosens. Bioelectron.* **2005**, *21*, 608−617.
(11) Cetó, X.; Gutiérrez, J. M.; Moreno-Barón, L.; Alegret, S.; del Valle, M. Voltammetric Electronic Tongue in the Analysis of Cava Wines. *Electroanalysis* **2011**, *23*, 72−78.
(12) Merolla, P. A.; Arthur, J. V.; Alvarez-Icaza, R.; Cassidy, A. S.; Sawada, J.; Akopyan, F.; Jackson, B. L.; Imam, N.; Guo, C.; Nakamura, Y.; et al. A Million Spiking-Neuron Integrated Circuit with a Scalable Communication Network and Interface. *Science* **2014**, *345*, 668−673.
(13) Davies, M.; Srinivasa, N.; Lin, T.-H.; Chinya, G.; Cao, Y.; Choday, S. H.; Dimou, G.; Joshi, P.; Imam, N.; Jain, S.; et al. Loihi: A Neuromorphic Manycore Processor with On-Chip Learning. *IEEE Micro* **2018**, *38*, 82−99.
(14) Imam, N.; Cleland, T. A. Rapid Online Learning and Robust Recall in a Neuromorphic Olfactory Circuit. *Nature Machine Intelligence* **2020**, *2*, 181−191.
(15) Han, J.-K.; Seo, M.; Kim, W.-K.; Kim, M.-S.; Kim, S.-Y.; Kim, M.-S.; Yun, G.-J.; Lee, G.-B.; Yu, J.-M.; Choi, Y.-K. Mimicry of Excitatory and Inhibitory Artificial Neuron With Leaky Integrate-and-Fire Function by a Single MOSFET. *IEEE Electron Device Lett.* **2020**, *41*, 208−211.
(16) Han, J.-K.; Oh, J.; Yun, G.-J.; Yoo, D.; Kim, M.-S.; Yu, J.-M.; Choi, S.-Y.; Choi, Y.-K. Cointegration of Single-Transistor Neurons and Synapses by Nanoscale CMOS Fabrication for Highly Scalable Neuromorphic Hardware. *Sci. Adv.* **2021**, *7*, eabg8836.
(17) Zhang, X.; Zhuo, Y.; Luo, Q.; Wu, Z.; Midya, R.; Wang, Z.; Song, W.; Wang, R.; Upadhyay, N. K.; Fang, Y.; et al. An Artificial Spiking Afferent Nerve Based on Mott Memristors for Neurorobotics. *Nat. Commun.* **2020**, *11*, 51.
(18) Wu, Q.; Dang, B.; Lu, C.; Xu, G.; Yang, G.; Wang, J.; Chuai, X.; Lu, N.; Geng, D.; Wang, H.; et al. Spike Encoding with Optic Sensory Neurons Enable a Pulse Coupled Neural Network for Ultraviolet Image Segmentation. *Nano Lett.* **2020**, *20*, 8015−8023.
(19) Han, J.-K.; Geum, D.-M.; Lee, M.-W.; Yu, J.-M.; Kim, S. K.; Kim, S.; Choi, Y.-K. Bioinspired Photoresponsive Single Transistor Neuron for a Neuromorphic Visual System. *Nano Lett.* **2020**, *20*, 8781−8788.
(20) Han, J.-K.; Sim, J.; Geum, D.-M.; Kim, S. K.; Yu, J.-M.; Kim, J.; Kim, S.; Choi, Y.-K.; Lee, M.-W.; Yu, J.-M.; Kim, S. K.; Kim, S.; Choi, Y.-K. 3D Stackable Broadband Photoresponsive InGaAs Biristor Neuron for a Neuromorphic Visual System with Near 1 V Operation. *2021 IEEE International Electron Device Meeting (IEDM)*; IEEE, 2021; pp 21.6.1−21.6.4, DOI: 10.1109/IEDM19574.2021.9720654.
(21) Miriyala, A.; Kessler, S.; Rind, F. C.; Wright, G. A. Burst Firing in Bee Gustatory Neurons Prevents Adaptation. *Curr. Biol.* **2018**, *28*, 1585−1594.
(22) Dahanukar, A.; Lei, Y.-T.; Kwon, J. Y.; Carlson, J. R. Two Gr Genes Underlie Sugar Reception in Drosophila. *Neuron* **2007**, *56*, 503−516.
(23) van der spiegel, J.; Lauks, I.; Chan, P.; Babic, D. The Extended Gate Chemically Sensitive Field Effect Transistor as Multi-Species Microprobe. *Sens. Actuators* **1983**, *4*, 291−298.
(24) Goda, T.; Miyahara, Y. Label-Free and Reagent-Less Protein Biosensing Using Aptamer-Modified Extended-Gate Field-Effect Transistors. *Biosens. Bioelectron.* **2013**, *45*, 89−94.
(25) Lee, M.-W.; Han, J.-K.; Yun, G.-J.; Yu, J.-M.; Lee, G.-B.; Han, S.-J.; Choi, Y.-K. A Temperature Sensor With a Thermillator. *IEEE Electron Device Lett.* **2021**, *42*, 1654−1657.
(26) Kwon, J.; Lee, B.-H.; Kim, S.-Y.; Park, J.-Y.; Bae, H.; Choi, Y.-K.; Ahn, J.-H. Nanoscale FET-Based Transduction toward Sensitive Extended-Gate Biosensors. *ACS Sensors* **2019**, *4*, 1724−1729.
(27) Kaisti, M.; Boeva, Z.; Koskinen, J.; Nieminen, S.; Bobacka, J.; Levon, K. Hand-Held Transistor Based Electrical and Multiplexed Chemical Sensing System. *ACS Sensors* **2016**, *1*, 1423−1431.
(28) Chen, S.; Bomer, J. G.; Carlen, E. T.; van den Berg, A. Al2O3/Silicon NanoISFET with Near Ideal Nernstian Response. *Nano Lett.* **2011**, *11*, 2334−2341.
(29) Charlu, S.; Wisotsky, Z.; Medina, A.; Dahanukar, A. Acid Sensing by Sweet and Bitter Taste Neurons in Drosophila Melanogaster. *Nat. Commun.* **2013**, *4*, 2042.
(30) Chiu, S.-W.; Wu, H.-C.; Chou, T.-I.; Chen, H.; Tang, K.-T. A Miniature Electronic Nose System Based on an MWNT−Polymer Microsensor Array and a Low-Power Signal-Processing Chip. *Anal. Bioanal. Chem.* **2014**, *406*, 3985−3994.
(31) Park, S.-C.; Jeong, H. J.; Heo, M.; Shin, J. H.; Ahn, J.-H. Carbon Nanotube-Based Ion-Sensitive Field-Effect Transistors with an On-Chip Reference Electrode Toward Wearable Sodium Sensing. *ACS Applied Electronic Materials* **2021**, *3*, 2580−2588.

(32) Ben Ali, M.; Jaffrezic-Renault, N.; Martelet, C.; Ben Ouada, H.; Davenas, J.; Charbonnier, M. Characterization of Copper Ion Sensing Thiacalix[4]Arene Films Evaporated on Semiconductor Substrates. *Materials Science and Engineering: C* **2001**, *14*, 17−23.

(33) Zhang, Y. V.; Ni, J.; Montell, C. The Molecular Basis for Attractive Salt-Taste Coding in Drosophila. *Science* **2013**, *340*, 1334−1338.

(34) Himmel, N.; Ziegler, M.; Mähne, H.; Thiem, S.; Winterfeld, H.; Kohlstedt, H. Memristive Device Based on a Depletion-Type SONOS Field Effect Transistor. *Semicond. Sci. Technol.* **2017**, *32*, 06LT01.

(35) Choi, H.-S.; Kim, H.; Lee, J.-H.; Park, B.-G.; Kim, Y. AND Flash Array Based on Charge Trap Flash for Implementation of Convolutional Neural Networks. *IEEE Electron Device Lett.* **2020**, *41*, 1653−1656.

https://doi.org/10.1021/acs.nanolett.2c01107
Nano Lett. 2022, 22, 5244−5251